ORNL/CP-95835

Pretest Fracture Evaluation of the NESC-1 Spinning-Cylinder Experiment*

J. A. Keeney B. R. Bass
P. T. Williams C. E. Pugh

Oak Ridge National Laboratory
P. O. Box 2009
Oak Ridge, TN, 37831-8056

Submitted for presentation at the
1998 ASME/JSME JOINT
PRESSURE VESSELS AND PIPING CONFERENCE
SAN DIEGO, CALIFORNIA
JULY 26-30, 1998

Abstract

This paper* describes a pretest fracture analysis of the cylinder specimen being used in the Network for Evaluating Steel Components (NESC) large-scale spinning-cylinder project (NESC-1). Organized as an international forum to exchange information on procedures for structural integrity assessment, to collaborate on specific projects, and to promote the harmonization of international standards, the NESC is currently focusing on a research project funded by United Kingdom Health and Safety Executive (HSE) to study the total process of structural integrity assessments of aged reactor pressure vessels (RPVs) containing subclad cracks. The intent is to have the problem studied by a wide range of organizations involved in RPV safety assessment. In this project, important safety assessment issues are being investigated by inspection and analysis of a spinning cylinder test which was performed at the AEA Technology facility at Risley, UK.

Thermo-elastic-plastic analyses were carried out for a clad cylinder model with a 74-mm-deep through-clad inner-surface crack. For this loading, the analytical results indicate that cleavage initiation may be achieved. The intervention of warm prestressing and loss of constraint may make cleavage initiation difficult to achieve in the heat-affected zone (HAZ) and near-HAZ regions.

1. Introduction

The Network for Evaluating Steel Components (NESC) is focusing on a research project funded by the United Kingdom Health and Safety Executive (HSE) to study the total process of structural integrity assessments of aged reactor pressure vessels (RPVs) containing subclad cracks. The intent is to have the problem studied by a wide range of organizations involved in RPV safety assessment. In this project, important safety assessment issues are being investigated by inspection and analysis of a spinning-cylinder test which was performed at the AEA Technology facility at Risley, UK.

The project consists of several phases. A thick cylinder was fabricated from A 508 B class 3 steel (inner diameter of 1.045 m; wall thickness of 175 mm including 4 mm of cladding; length of 1.3 m; and weight of 8 metric tons). The cylinder was heat treated with the aim of producing fracture toughness properties and residual stresses representative of those in the beltline region of an RPV after 30 years of service. Several cracks of varying sizes were inserted in the inner surface before the application of the stainless steel cladding. In the pretest phases of the project, the size and location of the subclad cracks were not revealed by the project management team or NESC management. Characterization blocks were fabricated in parallel with the cylinder for determination of tensile and fracture toughness properties of the cladding, heat-affected zone (HAZ), and base plate.

The cylinder was made available for inspection by teams using non-destructive examination (NDE) techniques. The teams employed methods used for in-service inspection of actual RPVs and applied them under conditions that were as realistic as possible. The findings of the inspection teams were reported to NESC management.

Other organizations participating in the NESC project performed pretest safety assessments of the cracks based on their interpretation of inspection results, specified pressurized-thermal-shock (PTS) loading, and materials property data. Results of these pretest assessments were also reported to NESC management.

The cylinder was fully instrumented and tested (on March 20, 1997) under simulated pressurized-thermal-shock loading in the spinning-cylinder test facility at Risley. Data from the test, including temperatures and rotational speeds, will be available for

* Research Sponsored by the Office of Nuclear Regulatory Research, U.S. Nuclear Regulatory Commission under Interagency Agreement 1886-8663-1W with the U.S. Department of Energy under Contract DE-AC05-96OR22464 with Lockheed Martin Energy Research Corp.

DISCLAIMER

posttest analysis. Following the test, the cylinder was made available to several international teams for inspection. Based on results of the posttest inspections, the safety assessments will be updated. The cylinder will then be destructively examined to determine the dimensions of the initial cracks and the extent of crack propagation during the test. Comparisons will be made between the pretest and posttest inspections and safety assessments and the observed size and evolution of the cracks.

This paper describes a pretest analysis of the NESC-1 experiment performed at the Oak Ridge National Laboratory and submitted to the NESC project management before the NESC-1 experiment. The analysis results are based on a NESC-1 problem definition prepared by the NESC Project.

2. Problem Definition

The cylinder specimen utilized in the analyses for NESC-1 has an inner diameter of 1045 mm, a wall thickness (including the cladding and clad HAZ) of 175 mm, clad thickness of 4 mm, HAZ thickness of 10 mm, and length of 1296 mm. The cylinder was fabricated from A 508 B class 3 steel with a clad overlay of 308 stainless steel. The most recent material properties are given in Table 1. These properties were provided by the NESC Task Group on Analysis and Task Group on Materials [1].

Analyses were carried out for an inner-surface through-clad crack with a crack depth of 74 mm and crack length of 200 mm, which is the best estimate of the geometry of the fatigued crack [2]. The loading conditions in the analyses consisted of the cylinder being heated to an initial temperature (T_i) of 290 °C, spun at increasing speed (maximum acceleration is 150 rpm/min) about its axial centerline up to a maximum speed of 2100 rpm, and then thermally-shocked on the inner surface with coolant at a temperature (T_c) of 5 °C to achieve cleavage crack initiation. During the thermal shock, the rotational speed of the cylinder is ramped up to a maximum speed of 2280 rpm. The analytical results were compared with material fracture toughness data taken from ref. 3 to predict whether the crack would tear ductilely and initiate in cleavage.

3. Fracture Analysis

3.1 Heat Conduction Model and Acceleration Profile

The calculation of the temperature distribution in the NESC-1 cylinder was performed with the ABAQUS [4] finite-element program — a nuclear quality assurance certified (NQA-1) code — using an axisymmetric model. The model consisted of 21 nodes and 10 axisymmetric 1-dimensional (1-D) conduction elements with convection boundary conditions. The geometry, material properties, and loading conditions were summarized in the previous section. Figure 1 shows the calculated transient temperature distribution in the cylinder.

The acceleration profile, as shown in Fig. 2, was begun at 2100 rpm with a maximum speed of approximately 2280 rpm being reached after 300 s.

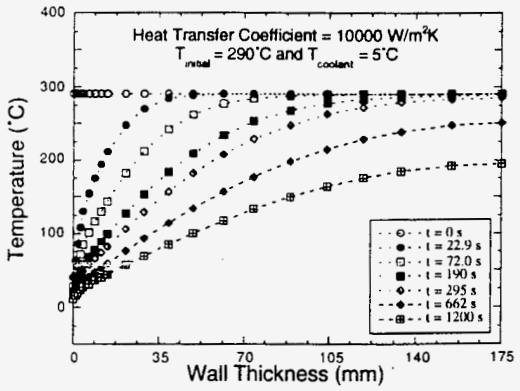

Fig. 1. Radial temperature distribution in the cylinder wall calculated by ABAQUS (T_i = 290°C).

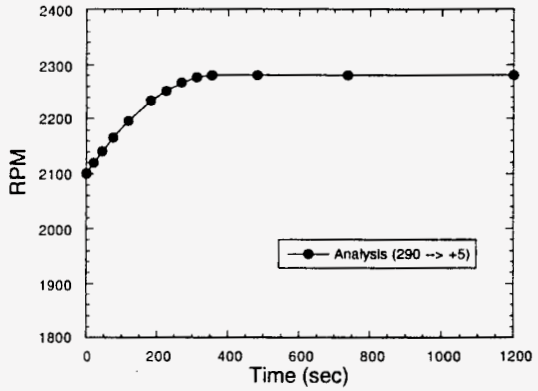

Fig. 2. Input acceleration profile.

3.2 Thermo-Elastic-Plastic Finite-Element Model

A model with a through-clad semi-elliptical axial crack at the inner surface having a crack length of 200 mm and crack depth of 74 mm was evaluated in this study. The clad HAZ thickness used in this model was 10 mm. The 3-D finite-element model of the cylinder was generated with the ORMGEN [5] mesh-generating program. From symmetry conditions, only one-fourth of the cylinder (180-degree model) is included in the model (Figs. 3 and 4). The model consists of 12,185 nodes and 2572 20-node isoparametric elements. A detailed plot of the crack-tip region is shown in Fig. 4.

The cylinder was analyzed with the ABAQUS [4] finite-element program, which employs a domain integral method for the computation of the J-integral. Values for K_J were calculated from the J-integral using the following plane-strain relation:

$$K_J = \sqrt{\left(\frac{E}{1-\nu^2}\right) J} \qquad (1)$$

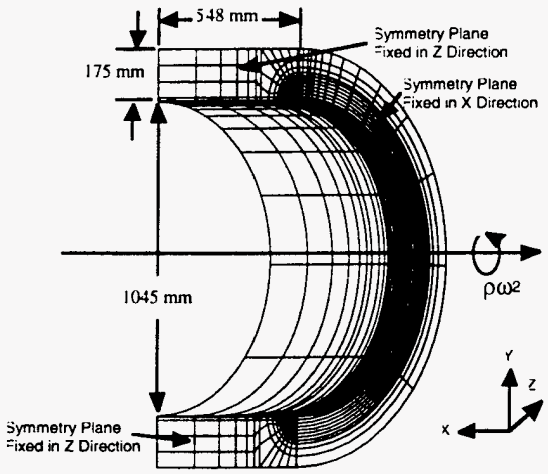

Fig. 3. Three-dimensional finite-element model of the clad cylinder (NESC-1) with a 74-mm-deep through-clad crack.

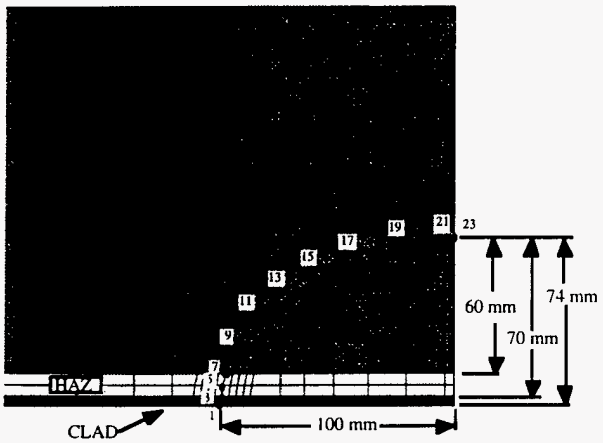

Fig. 4. Crack-tip region of the cylinder model.

where Young's modulus E = 206.0 GPa and Poisson's ratio ν = 0.28 for the base and HAZ materials, and E = 147.0 GPa, ν = 0.30 for the clad material. The thermo-elastic-plastic analyses were performed using the material properties in Table 1 and the stress-plastic strain curves depicted in Fig. 5. The temperatures through the wall for each time step were obtained from the heat conduction analysis and mapped onto the 3-D cylinder model. The "stress-free" temperature was taken as the initial temperature (before thermal shock) of the cylinder; i.e., residual stress effects were ignored.

3.3 Analysis Results

The time history of the crack-mouth opening displacement (CMOD) is shown in Fig. 6. The value of CMOD reaches its peak value of 1.3 mm at 311 s into the transient. The hoop stress and effective stress are plotted through the wall thickness at various times in the transient in Figs. 7 and 8, respectively. The axial position for these stresses is 202 mm from the end of the crack or 302 mm from the midplane (symmetry plane) of the vessel.

Time histories of the J-integral for four points near the inner surface (see Fig. 4 for these locations) are plotted in Fig. 9. The highest J-integral values are at the middle of the HAZ. The J-integral values for the two interface positions are approximately the same. The J-integral data are also plotted as a function of crack-front angle (see Fig. 10) for four different times in the transient (0, 120, 226, and 311 s). Values of K_J are plotted and discussed in Section 3.4.

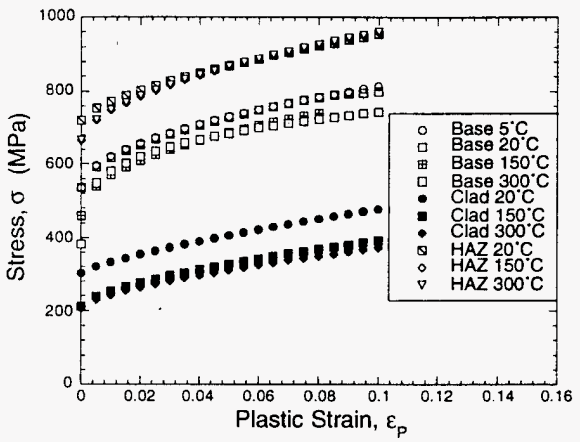

Fig. 5. Multilinear representations of the stress-plastic strain behavior for A 508 B base forging, 308 stainless steel clad, and HAZ materials.

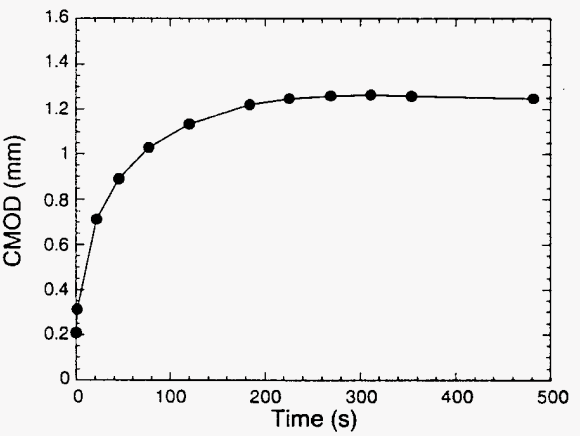

Fig. 6. Time history of CMOD.

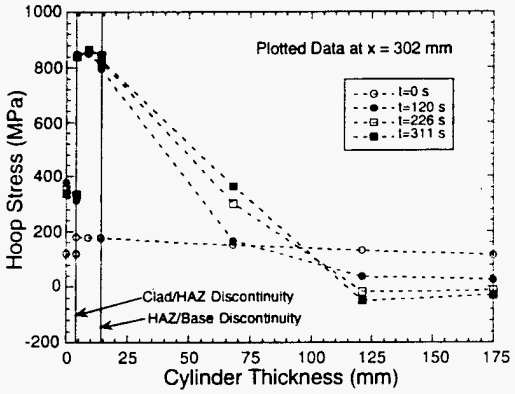

Fig. 7. Hoop stress distribution through the wall at various times in the transient.

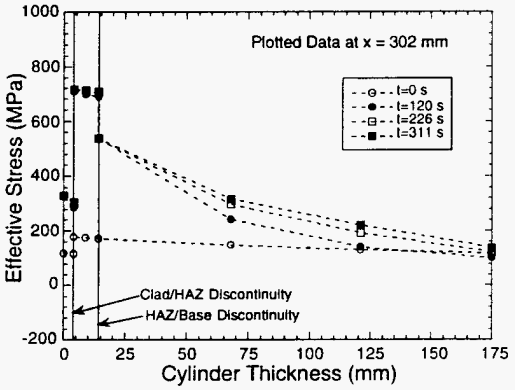

Fig. 8. Effective stress distribution through the wall at various times in the transient.

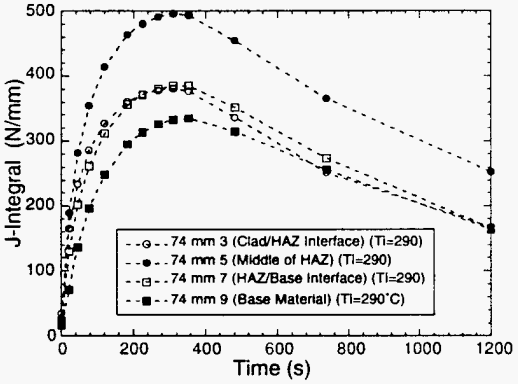

Fig. 9. Time histories of J-integral.

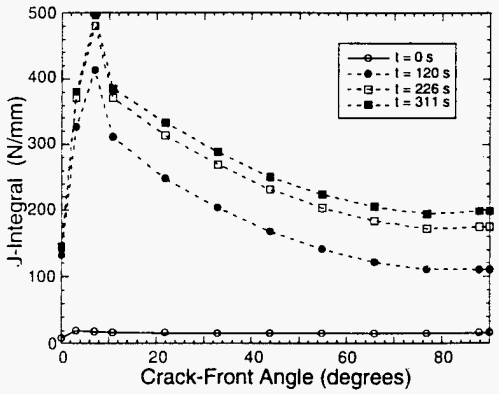

Fig. 10. J-integral versus crack-front angle.

3.4 K_J Evaluation

K_J was calculated at several nodal positions along the crack front. Values are plotted as a function of temperature for positions 7 and 9 around the crack front (see Fig. 4 for these locations) in Fig. 11. The K_J values for the HAZ/Base interface (position 7) peak at 311 s with a value of 294 MPa$\sqrt{m}$. The K_J values in the base material (position 9) are lower than the interface (peak K_J of 274 MPa$\sqrt{m}$ at 354 s). The values of K_J are compared with the measured cleavage fracture toughness values and fracture resistance values for the base material from ref. 3. Ductile tearing is predicted to begin after about 20 to 50 s. For both locations, there is a substantial amount of ductile tearing (~2 to 3 mm) followed by cleavage initiation at ~120 s at the interface and ~226 s in the base metal.

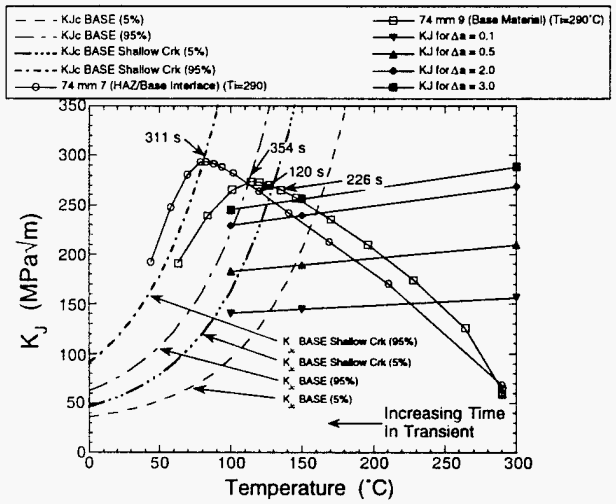

Fig. 11. Comparison of K_J values with material toughness for base material.

The crack peak K_J values occurred in the middle of the HAZ (see Fig. 12), but $\frac{dK}{dt}$ becomes negative (warm-prestress effects [6, 7]) shortly after the crack becomes critical ($K_J/K_{Jc} > 1$ beyond

the HAZ toughness curve). The peak K_J value at the clad/HAZ interface is lower, but $\frac{dK}{dt}$ is positive. In both cases, constraint effects are an issue. Loss of constraint in this area would hinder cleavage initiation.

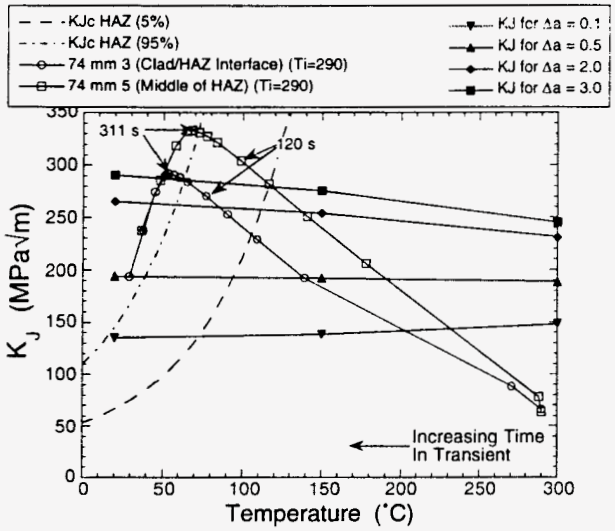

Fig. 12. Comparison of K_J values with material toughness for HAZ material.

3.5 Crack Growth Evaluation

Subclad crack growth was modeled in the cylinder by generating three additional models where the crack half-length was set at 106, 112, and 128 mm, producing crack extensions of 6, 12, and 28 mm, respectively. To model tunneling of the crack under the intact cladding layer, the cladding nodes over the extending crack were restrained against opening over a distance from the initial crack length (100 mm) to where the crack extended. The K_J v. temperature curves at mid-HAZ are plotted in Fig. 13 for each model. Contour plots of the hoop strains on the inner surface of the cylinder are shown in Figs. 14-17 for each model at 311 s (the time of maximum crack driving force). These plots illustrate that the peak hoop strains occur in regions which are offset from the plane of the crack.

4. Summary and Conclusions

Thermo-elastic-plastic analyses were carried out for a clad cylinder model with a 74-mm-deep through-clad inner-surface crack. For this loading, the analytical results indicate that cleavage initiation may be achieved. The intervention of warm prestressing and loss of constraint may make cleavage initiation difficult to achieve in the HAZ and near-HAZ regions. The failure assessment is summarized in Table 2.

References

1. D. McGarry, NESC, *TG3 Final Calculations*, letter to all TG3 members, October 4, 1996.

2. B. R. Bass, *Report of Foreign Travel of B. R. Bass, Computational Physics and Engineering Division*, USNRC Foreign Trip Report, ORNL/FTR-5948, Lockheed Martin Energy Research Corp., Oak Ridge National Laboratory, October 11, 1996.

3. R. Rintamaa, NESC-1 Spinning-Cylinder Project – Materials Task Group (TG2), *Summary of Material Property Data*, Revised 23.11.1996, November 12-13, 1996.

4. *ABAQUS Theory Manual, Version 5.5*, Hibbit, Karlson and Sorensen, Inc., Providence, RI, 1996.

5. B. R. Bass and J. W. Bryson, Jr., *Applications of Energy Release Rate Techniques to Part-Through Cracks in Plates and Cylinders, Volume 1, ORMGEN-3D: A Finite Element Mesh Generator for 3-Dimensional Crack Geometries*, USNRC Report NUREG/CR-2997/V1 (ORNL/TM-8527), Union Carbide Corporation Nuclear Division, Oak Ridge National Laboratory, December 1982.

6. J. A. Keeney and B. R. Bass, *Analyses of the Reconstituted NESC-1 Spinning-Cylinder Experiment*, USNRC Letter Report ORNL/NRC/LTR-94/25, Martin Marietta Energy Systems, Inc., Oak Ridge National Laboratory, August 31, 1994.

7. R. H. Bryan et al., *Pressurized-Thermal-Shock Test of 6-in.-Thick Pressure Vessels. PTSE-1: Investigation of Warm Prestressing and Upper-Shelf Arrest*, USNRC Report NUREG/CR-4106 (ORNL-6135), Martin Marietta Energy Systems, Inc., Oak Ridge National Laboratory, April 1985.

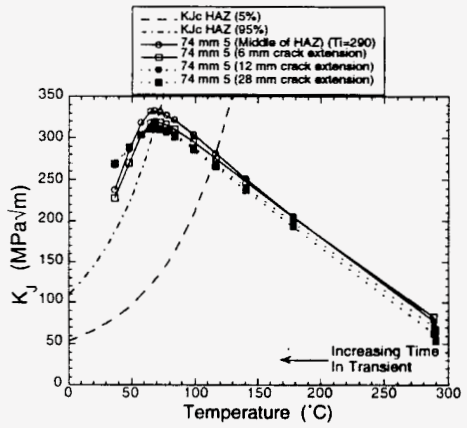

Fig. 13. Comparison of K_J values from various crack extension models with material toughness for HAZ material.

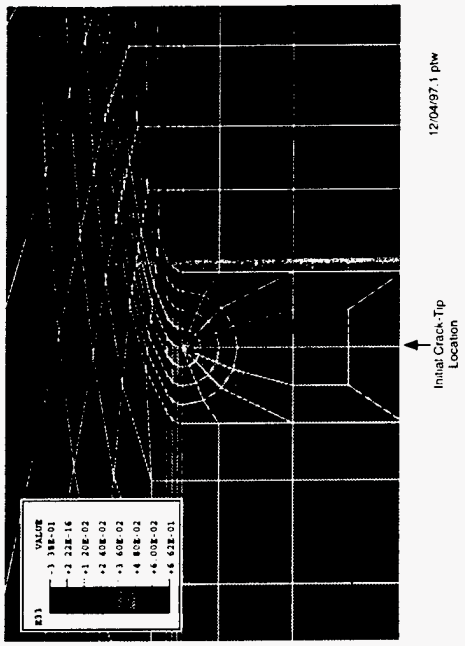

Fig. 14. Contours of hoop strain on the cylinder inner surface (no crack extension).

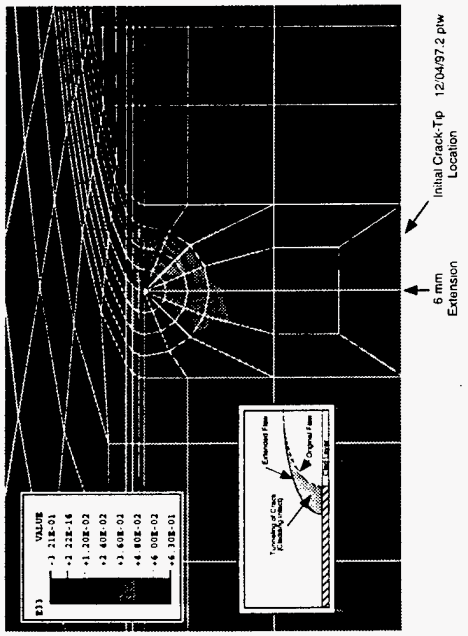

Fig. 15. Contours of hoop strain on the cylinder inner surface (6 mm crack extension).

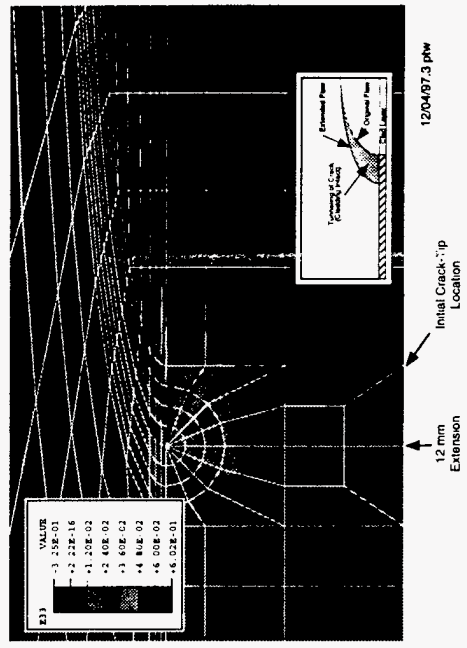

Fig. 16. Contours of hoop strain on the cylinder inner surface (12 mm crack extension).

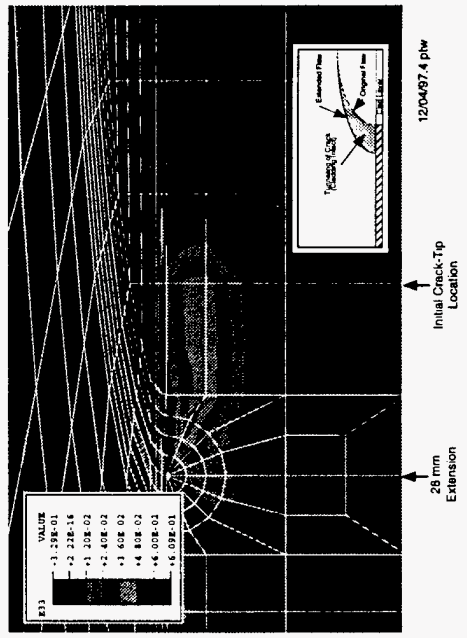

Fig. 17. Contours of hoop strain on the cylinder inner surface (28 mm crack extension).

Table 1. Material properties for NESC-1 analyses

Material Property	A508 Base Forging	HAZ	Stainless Steel Cladding
Thermal Conductivity (k), W/m-K	40.26 @ 25°C 40.93 @ 150°C 39.68 @ 250°C 37.24 @ 350°C	40.26 @ 25°C 40.93 @ 150°C 39.68 @ 250°C 37.24 @ 350°C	13.34 @ 25°C 15.90 @ 150°C 18.15 @ 250°C 20.10 @ 350°C
Specific Heat (c_p), J/kg-K	4.1E-04T+0.432	4.1E-04T+0.432	4.1E-04T+0.432
Density (ρ), kg/m^3	7800 @ 20°C 7750 @ 290°C	7800 @ 20°C 7750 @ 290°C	7800 @ 20°C 7750 @ 290°C
Young's Modulus (E), GPa	211.7–0.0682T	211.7–0.0682T	150.2–0.0862T
Coefficient of Thermal Expansion (α), °C^{-1}	1.27E-05 @ 75°C 1.40E-05 @ 175°C 1.56E-05 @ 275°C	1.27E-05 @ 75°C 1.40E-05 @ 175°C 1.56E-05 @ 275°C	1.67E-05 @ 100°C 1.73E-05 @ 200°C 1.95E-05 @ 300°C
Poisson's Ratio (ν)	0.28	0.28	0.30
Yield Stress (σ_y), MPa	535.0 @ 5°C 536.7 @ 20°C 458.6 @ 150°C 381.9 @ 300°C	720.0 @ 20°C 665.0 @ 150°C 665.0 @ 300°C	302.6 @ 20°C 212.0 @ 150°C 205.7 @ 300°C
Heat transfer coefficient : 10,000 W/m^2-K (inner surface)			

Table 2. Failure Assessment

Location	Ductile Tearing		Cleavage Initiation
	time (s)	Δa (mm)	time (s)
Base (near HAZ)	33.5	4	226.0(50%)
HAZ/Base Interface	17.6	3	93.50 (50%) 152 (95%)

Report Number (14) ORNL/CP-95830
CONF-980708--

Publ. Date (11) 199712

Sponsor Code (18) DOE/ER, XF

JC Category (19) UC-940, UC-600, DOE/ER

DOE